Articles

Starch-Coated Superparamagnetic Nanoparticles as MR Contrast Agents

Do Kyung Kim,*,† Maria Mikhaylova,† Fu Hua Wang,‡ Jan Kehr,‡ Börje Bjelke,§ Yu Zhang,† Thomas Tsakalakos,|| and Mamoun Muhammed†

Materials Chemistry Division, Royal Institute of Technology, SE-100 44 Stockholm, Sweden, Department of Neuroscience, Karolinska Institutet, SE-171 77, Stockholm, Sweden, Department of Radiology, Center for Surgical Sciences, Huddinge University Hospital, Karolinska Institutet, SE-141 86 Stockholm, Sweden, and Laboratory for Nanostructured Materials Research, Department of Ceramics, Rutgers University, Piscataway, New Jersey 08854

Received June 26, 2003. Revised Manuscript Received August 22, 2003

Superparamagnetic iron oxide nanoparticles (SPION) with suitable bio-compatible coatings have been used in biomedicine, particularly in magnetic resonance imaging (MRI), tissue engineering, and drug delivery applications. In this study, we describe the synthesis of SPION and its use for experimental in-vivo applications in MRI. SPION with a mean size of 6 nm have been prepared under inert atmosphere, in a polymeric starch matrix, by controlled chemical coprecipitation of magnetite phase from aqueous solutions containing suitable salts of Fe^{2+} and Fe^{3+}. X-ray powder diffraction was used to confirm a pure magnetite phase for the SPION. The influence of oxidizing agents on the cleavage of the starch chains was investigated by changing the concentration of H_2O_2. An aqueous solution of H_2O_2/NaOH cleaves the glycosidic bonds and reduces the polymer chains to a critical average molecular weight. From the dynamic light scattering (DLS) size distribution, the bulk agglomeration size was decreased by approximately 50% of the bulk size when treated by H_2O_2. Freshly synthesized starch-coated SPION in buffered artificial cerebro-spinal fluid were injected into the brain parenchyma of anaesthetized rats for in-vivo monitoring. Analysis of T_2*-weighted images and T_2*-maps revealed formation of a concentration gradient for the SPION at the injection site, indicating SPION dispersion in the living brain parenchyma from the center of the injection site toward the periphery. The starch-coated SPION show a biocompatibility and possibility of being transported in the extracellular space as well as being internalized in nerve cells.

1. Introduction

The presently described nonselective superparamagnetic iron oxide nanoparticles (SPION) represent an efficient and valuable source of exogenous T_2 contrast agent which has become an important and indispensable tool for enhancing the sensitivity in tissue discrimination of biological processes using MRI. The efficiency of these agents has been proven useful in early detection of tumors, lymph node metastasis, and liver sclerosis, or in experimental functional magnetic resonance imaging (fMRI).[1] When dextran was used as a coating agent for SPION, thus forming a core of iron oxide and a coating of biocompatible dextran. The size of the core affects the sensitivity of detection in MRI and the overall size can be modified by varying the thickness of the dextran layer giving the nanoparticle possibilities of extracellular transport or restricting it to the intravascular compartment. This type of nanoparticle have been on the market and several studies have shown that it can be successfully used in cancer diagnostics in liver tumors and pathologies where SPION are selectively taken up by healthy liver cells while sclerotic parts of the liver cannot.[2] Consequently, in MRI the healthy regions are darkened and the diseased regions remain bright. The general tendency is to develop MRI devices with higher magnetic field strength for in-vivo applications, which give the opportunity for faster recordings at higher spatial resolution.

* To whom correspondence should be addressed. E-mail: kyung@matchem.kth.se or mamoun@matchem.kth.se.
† Royal Institute of Technology.
‡ Department of Neuroscience, Karolinska Institutet.
§ Center for Surgical Sciences, Karolinska Institutet.
|| Rutgers University.

(1) Abo, M.; Chen, Z.; Lai, L. J.; Reese, T.; Bjelke, B. *NeuroReport* **2001**, *12*, 1543.

(2) (a) Van Beers, B. E.; Sempoux, C.; Materne, R.; Delos, M.; Smith, A. M. *J. Magn. Reson. Imaging* **2001**, *13*, 594. (b) Van Beers, B. E.; Gallez, B.; Pringot, J. *Radiology* **1997**, *203*, 297.

10.1021/cm031104m CCC: $25.00
Published on Web 10/04/2003

An increasing interest for these SPION is in tracking molecules and cells, which have been proven to function in platelets[3], and even more interesting is their use for the labeling of stem cells or *T*-lymphocytes which are shown for in vivo[4] tracing of testicular inflammatory reactions in rats. SPION labeled *T*-cells in the blood pool were, in a large number, immunologically attracted to the inflamed rat's testicles and caused thereby a decrease in the MRI signal. Alternatively, antibody-conjugated SPION can serve as a target-selective magnetic resonance contrast agent and has been used commercially in vitro for cell sorting.[5] Magnetoliposomes is another approach which has been successfully used for cell labeling in which PEG-modified magnetoliposomes, with a diameter of 40 nm containing 1−6 SPION crystals per vesicle, were found to have excellent properties as a MR contrast agent for bone marrow enhancement.[6] Colloidal processing of magnetic nanoparticles has been extensively studied, emphasizing the characteristics for dispersing SPION as a ferrofluid. To maintain SPION in a colloidal solution the attractive forces from the SPION must be considered, such as van der Waals' forces and magnetic dipole−dipole interactions generated from remnant magnetic forces, which tend to agglomerate the particles. These forces must be stronger than the attractive forces in order to stabilize the ferrofluid in a colloidal solution. Surfactants are typically introduced to modify the surface properties, while Coulombic repulsion accounts for the stability in ionic ferrofluids.[7]

Such colloidal magnetic particles have recently been used in many important applications, including MR imaging and magnetically guided drug delivery.[8] Specifically, MRI approaches using contrast agents are being used to increase conspicuity of adjacent internal organs and tissue.[9] The sensitivity of detection and delineation of pathological structures, such as primary and metastatic brain tumors, inflammation, and ischemia have been improved by introducing contrast agents. Potential candidates of biomaterials as drug carriers and coating agents for MR purposes can be natural polymers such as carbohydrates and proteins. Starch, a long-chain polymer of D-glucose, is one of the most abundant naturally occurring polysaccharides. It has been used experimentally as a drug carrier because of its biocompatibility, biodegradability, and nontoxicity.

A controlled coprecipitation approach has been developed for the synthesis of SPION with a mean size of 6 nm.[10] This paper is focused on coating magnetic cores with biocompatible outer shells. In addition, the application of the biocompatible starch-coated SPION has been investigated in vivo in a rat brain by MR imaging.

Table 1. Influence of Oxidizing Agent H_2O_2 on the Cluster Size of SPION Embedded in Polymeric Starch Matrix

sample	SPION (mg/mL)[a]	H_2O_2[a]	particle size by DLS[b] (nm)
S1	0.5	0	87
S2	0.476	0.022	83
S3	0.456	0.042	73
S4	0.435	0.06	47
S5	0.417	0.076	42
S6	0.4	0.092	69

[a] Final concentrations of the samples. [b] DLS, Dynamic light scattering.

2. Experimental Section

Chemicals and Solutions. All the chemicals were of reagent grade and used without further purification. Ferric chloride hexahydrate ($FeCl_3 \cdot 6H_2O$, >99%), ferrous chloride tetrahydrate ($FeCl_2 \cdot 4H_2O$, >99%), and starch (25−30 KDa, $(C_6H_{10}O_5)_n$, >99%) were obtained from Aldrich. For particle coating we used potato starch containing quaternary ammonium groups (2-hydroxy-3-trimethylammonium-propyl starch) at the degree of substitution (DS) of 0.352. Hydrogen peroxide (H_2O_2, >99%) and hydrochloric acid (HCl, >37%) were obtained from KEBO. Milli-Q water was re-deionized (specific conductance < 0.1 s/cm) and deoxygenated by bubbling with N_2 gas for 1 h prior to use. In addition, various amounts of starch were dissolved in 100 mL of deionized water at 90 °C. After the starch was thoroughly dissolved, the starch solution was immediately placed in a 60 °C water bath.

Stock solutions of 1.28 M $FeCl_3 \cdot 6H_2O$, 0.64 M $FeCl_2 \cdot 4H_2O$, and 0.4 M HCl were prepared as a iron source by dissolving the respective chemicals in Milli-Q water under stirring. Stock solutions of 0.9−1.5 M NaOH were prepared as alkali sources in the same way. A solution of 1×10^{-2} M HCl was prepared for surface neutralization. NaCl solutions (5×10^{-3} M and 1×10^{-2} M) were prepared as background electrolyte solutions.

Synthesis. A dispersion of SPION was prepared by alkalinizing an aqueous mixture of ferric and ferrous salts with NaOH at room temperature. N_2 gas was bubbled through the reaction medium during synthesis in a closed system. The detailed procedure of this controlled coprecipitation approach has been reported elsewhere.[11]

A specific amount of the Fe stock solutions was poured into a prepared starch solution under vigorous stirring. A 25-mL portion of the starch and iron mixture was then added dropwise into 200 mL of 1.0 M NaOH under vigorous mechanical stirring (2000 min^{-1}) at 60 °C for 2 h. Around 50 wt % of water was evaporated during the boiling. The remaining suspension was cooled to room temperature within 12 h. The gels formed were washed with deionized water until the pH was lowered to less than 8.5. Starch-coated iron oxide particles were dialyzed for the removal of excess unreacted starch at 37 °C for 2−3 days while being continuously stirred.

A suspension of 120 mL containing of 0.5 mg/mL SPION embedded in starch was divided into six 20-mL samples (designated S1−S6). The mean size distribution of fraction S1 before the treatment with H_2O_2 was 87 nm. Varying volumes (1−5 mL) of 0.46 M H_2O_2 was mixed with the 20-mL samples of starch-coated SPION (S2−S6). More detailed information on final concentrations is summarized in Table 1.

Characterization. *XRD Measurement.* Crystallographic analysis of the samples was performed by powder X-ray diffraction (XRD). Diffraction patterns of intensity vs 2θ were recorded with a Philips PW 1830 diffractometer, using a

(3) Johansson, L. O.; Bjørnerud, A.; Ahlström, H. K.; Ladd, D. L.; Fujii, D. K. *J. Magn. Reson. Imaging* **2001**, *13*, 615.
(4) Perez, J. M.; Josephson, L.; O'Loughlin, T.; Högemann, D.; Weissleder, R. *Nature Biotechnol.* **2002**, *20*, 816.
(5) (a) Manent, J.; Oguievetskaia, K.; Bayer, J.; Ratner, N.; Giovannini, M. *J. Neurosci. Methods* **2003**, *123*, 167. (b) Zigeuner, R. E.; Riesenberg, R.; Pohla, H.; Hofstetter, A.; Oberneder, R. *J. Urol.* **2003**, *169*, 701. (c) Meier, D.; Schachner, M. *J. Neurosci. Res.* **1982**, *7*, 135.
(6) Bulte, J. W. M.; Cuyper, M.; Despres, D.; Frank, J. A. *J. Magn. Magn. Mater.* **1999**, *194*, 204.
(7) Sjöholm, I.; Laakso, T.; Stjärnkvist, P. *J. Pharm. Sci.* **1987**, *76*, 134.
(8) Zimmer, C.; Wright, S. C., Jr.; Engelhardt, R. T.; Johnson, G. A.; Kramm, C.; Breakefield, X. O.; Weissleder, R. *Exp. Neurol.* **1997**, *143*, 61.
(9) Roberts, T. P. L.; Shuang, N.; Roberts, H. C. *Eur. J. Radiol.* **2000**, *34*, 166.
(10) Kim, D. K.; Zhang, Y.; Kehr, J.; Klason, T.; Bjelke, B.; Muhammed, M. *J. Magn. Magn. Mater.* **2001**, *225* (1−2), 256.
(11) (a) Massart, R.; Cabuil, V. *J., Phys. Chem.* **1987**, *84*, 967. (b) Granqvist, C. G.; Buhrman, R. H. *J. Appl. Phys.* **1976**, *47*, 2200.

monochromatized X-ray beam with nickel-filtered Cu Kα radiation ($\lambda = 1.5418$ Å). A continuous scan mode was used to collect 2θ data from 20 to 70° with a 0.02 sample pitch and a 4° min^{-1} scan rate. X-ray tube voltage and current were set at 40 kV and 35 mA, respectively. The average crystalline sizes of the sample were estimated using Debye−Scherrer's formula[8] from the full width at half-maximum (fwhm) of main intense peak.

TEM Measurement. A TEM study was carried out on a JEOL-2000EX microscope with an electron kinetic energy of 200 kV. The specimen for TEM imaging was prepared from the SPION suspension in deionized water by using sonication for 3 min. After sonication, 1 mL of the SPION suspension was centrifuged for 5 min at 14 000 min^{-1}. A drop of well-dispersed supernatant was placed on a carbon-coated 200 mesh copper grid, followed by drying the sample at ambient conditions before it was attached to the sample holder on the microscope. The particle size and size distribution were calculated from TEM images for all prepared samples using an image analysis program by measuring the diameters of at least 500 particles.

FTIR Measurement. Chemical bonding information on metal−oxygen, hydroxyl, and other functional groups was obtained by use of Fourier transform infrared spectroscopy (FTIR, Avatar 360, Nicolet) using the Smart DuraSamplIR Diamond ATR Accessory. Each spectrum was collected after 32 scans at a resolution of 1 cm^{-1}.

Particle Size Measurement. The particle size distribution was measured using a Brookhaven BI-XDC instrument by measuring the rate of sedimentation under applied centrifugal force based on X-ray absorption and by using a BI-90 particle sizer based on dynamic light scattering (DLS).

ξ-Potential Measurement. The ξ-potential of the starch-coated SPION was measured in 5 mM and 10 mM NaCl background electrolyte solutions using a Zetasizer 2000 (Malvern Instrument Ltd.). The test suspensions were prepared at fixed concentrations in buffer solutions, each adjusted to a given pH with NaOH or HCl stock solutions.

ESA Measurement. In situ monitoring of the SPION co-precipitation reaction in a starch matrix was measured with a Matec Applied Sciences (ESA-9800) system. The dynamic mobility, also called the acoustic pressure amplitude (ESA), was generated by colloidal particles in alternating high-frequency electric fields, following the formula

$$ESA = c \times \Delta\rho \times \Phi \times \mu(\omega) \tag{1}$$

where c is the sound velocity in the dispersing liquid, $\Delta\rho$ is the difference between the solid and liquid density, Φ is the volume fraction of the solid phase in the dispersion, and μ is the dynamic mobility. The dynamic mobility was calculated from the equation

$$\mu = \frac{2\xi\epsilon}{3\eta} G[1 + \gamma f(\kappa a)] \tag{2}$$

where ξ is the zeta potential, ϵ is the dielectric constant of the medium, η is the viscosity of the dispersion, and γ is an inertial term that is a function of the amplitude and phase of the acoustic signal. G is a geometrical factor for a given electrode geometry and is constant for a set of experiments. The term in brackets contains γ, which depends on the conductivity of the solution and of the particles, and the function $f(\kappa a)$, where κ is the reciprocal value of the Debye length and a is the curvature radius of the double layer.

An aliquot of 250 mL of 1.0 M NaOH solution was placed in a Teflon sample container. Iron stock solution (1 mL) was pumped by a MICROLAB 500 Digital buret and stabilized for 10 s before measurements were taken. The electro-acoustic signal, electrical conductivity, and temperature were recorded as a function of pH while using the titration cell. The stirring speed was kept at a maximum value.

MR Imaging in the Rat Brain. This study was performed according to animal care legislation and approved by the local animal ethical committee. The study was performed on 8 rats, which were divided into two groups and subjected to different analysis systems, i.e., MRI and morphology. Male Sprague−Dawley rats (200−250 g, $n = 8$, B&K Universal, Stockholm, Sweden) were kept under standardized conditions concerning day night cycle, temperature, and humidity, with free access to food and water. For analysis, each rat was anesthetized with isoflurane (Abbott, Sweden) in air. Body temperature was monitored by a rectal probe and maintained at 37.0−38.0 °C by use of an auto-regulated heating pad during the surgery. During the MR recording, the body temperature was maintained by a warm air stream. Under anesthesia, a sagital skin incision was made over the skull, and a 1-mm hole was drilled into the skull approximately 1.0 mm posterior and 2.5 mm bilateral to the bregma. SPION (42 nm (S5)) was selected to be injected into rat brain. A Hamilton 10-μL glass syringe (Hamilton, Reno, NV) was then used to inject 0.3 μL of SPION (approximately 0.05 mg/mL SPION) into the striatum at a depth of 4 mm from the dural surface. The injection was made over 1 min, and the needle was withdrawn over 5 min. MRI scanning was performed 1 h after the injection of SPION suspension into the brain.

MRI measurements were carried out using a 4.7 T superconducting magnet (Biospec Avance 47/40, Bruker, Karlsruhe, Germany) equipped with a 12-cm self-shielded gradient system in combination with a purpose-built semi-circular RF resonator of 35-mm i.d. The rat's head was placed inside the coil in a prone position with its body properly supported within a purpose-built plastic cradle. To visualize the localization of the SPION a standard Bruker gradient echo (GEFI) sequence was modified to allow multi-echo acquisitions. Such a sequence is sensitive to the susceptibility changes in the tissue created by the presence of superparamagnetic particles.[12]

The rats were processed for morphological analysis 1 day after the injection of SPION. Under deep anesthesia, (Pentobarbital 50 mg/kg) the rats were perfused with 4% formalin whereafter the brains were removed and kept refrigerated in the fixative until further processed for morphological evaluation. Coronal, 50-μm thick, vibratom sections were cut from the injection site. The sections were glass-mounted and Nissl stained with Thionin, according to standard techniques. Microscopic evaluation and photographic documentation were performed using a Nikon microscope.

3. Results

Figure 1 shows a TEM image that was used to determine particle size distribution and morphology. Spherical or ellipsoidal particles consisting of a SPION core and a diameter around 7.2 nm were found. However, it was evident that the SPION were distributed homogeneously in the polymeric matrix.

From the XRD measurements with the line broadening of the SPION diffraction peak, the particle size of 6 nm was calculated for SPION.

The nucleation speed per unit area was isotropic at the interface between the SPION, which resulted in final spherical shapes. The size distribution was calculated using the following equation, based on a log-normal function[10] and image analysis program:

$$p(D) = \frac{1}{D\sigma_d\sqrt{2\pi}} \exp\left(-\frac{1}{2\sigma_d{}^2}\left(\ln\frac{D}{D_0}\right)^2\right) \tag{3}$$

where σ_d is the diameter standard deviation and D_0 is the mean diameter. These results hold for a volumetric standard deviation of $\sigma_v = 3\sigma_d$ and a mean volume of

(12) Rinck, P. A.; Muller, R. N.; Petersen S. B. *Magnetic Resonance in Medicine. The Basic Textbook of the European Magnetic Resonance Forum*. Blackwell Scientific Publications: Cambridge, MA, 2001;ISBN 0632-03781-4.

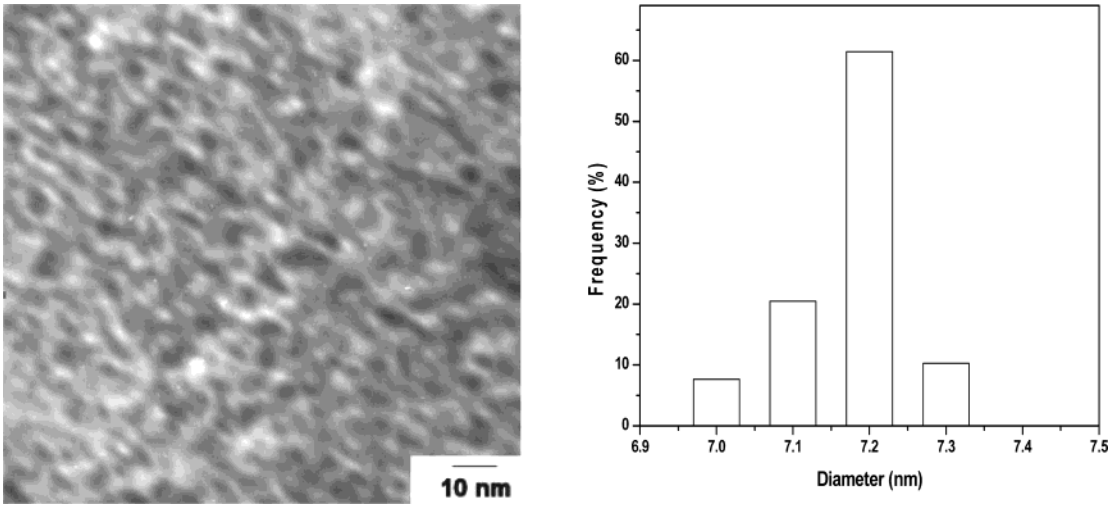

Figure 1. Transmission electron microscopy image (left) and the corresponding particle size histograms (right) of SPION swelled in starch polymeric matrix prepared by controlled coprecipitation.

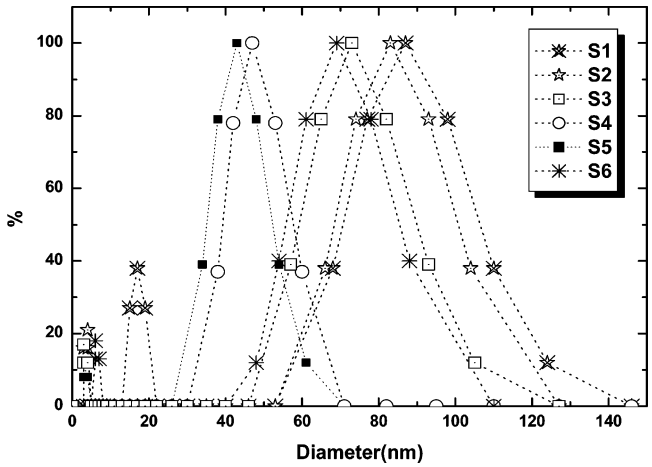

Figure 2. Particle size distributions of different samples of SPION embedded in starch after treated with different H_2O_2 concentrations.

$V_0 = (\pi/6)D_0^3$. The particle size, determined by eq 3 was 7.2 nm with a standard deviation of $\sigma_d = 0.2$ (Figure 1), which is in agreement with the crystal size of 6 nm calculated from the XRD data.

The effect of oxidizing agent, used for the cleavage of the polymeric starch chains on the final size distributions of the starch-coated SPION, is shown in Figure 2 and summarized in Table 1. The results of the particle size analysis of the TEM images of starch-coated SPION (S1−S6) revealed that the observed size distribution was for the agglomerated clusters rather than for the individual particles. Following the treatment with H_2O_2, the average cluster size decreased from 87 nm (S1) to the smallest size of 42 nm (S5). Further addition of H_2O_2 caused an increase of the cluster size (S6, 69 nm).

Figure 3 shows the results of ESA and conductivity measurements from the SPION formation in the presence of polymeric starch matrix. Each data point represents 1 mL of iron source in the starch matrix which was delivered into the reaction chamber. After a 10-s stabilization period, the in-situ reaction monitoring was initiated, providing indirect information on the precipitation reaction mechanism. The precipitation reaction started at a pH of 12.8 with an ESA value of 1.45 mPa·M/V. The results show that the conductivity

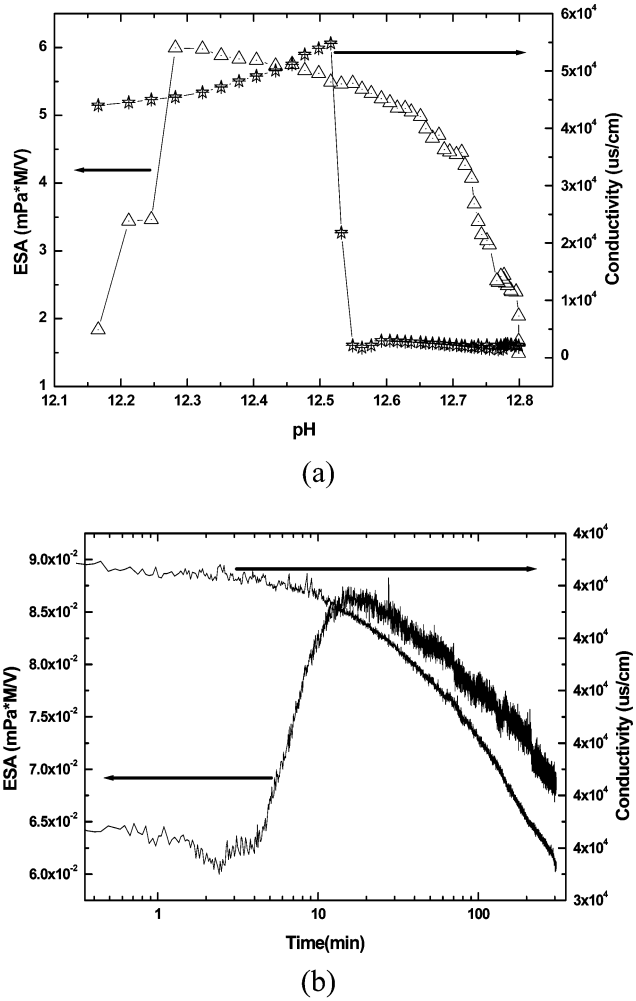

Figure 3. In situ surface charge monitoring of SPION precipitation polymeric starch matrix: (a) ESA results of the effects of pH dependence, and (b) long-term stability measurements for 300 min.

did not change until the pH reached 12.55, afterward the conductivity dramatically increased by a factor of 4. Stoichiometric amounts of iron source and a 20% excess amount of alkali were used for SPION precipitation reaction. The byproduct (NaCl) of the neutralization reaction acts as a background electrolyte, causing an

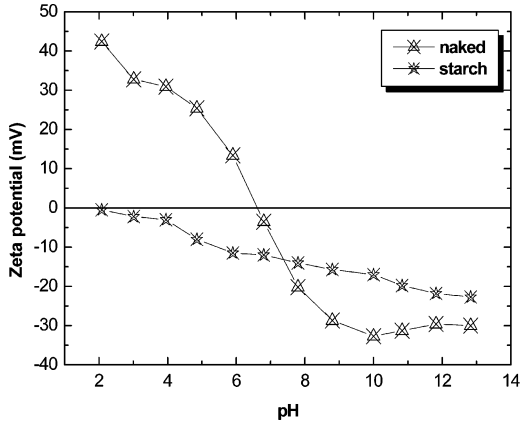

Figure 4. Microelectrophoretic measurements of dilute uncoated and starch-coated SPION suspensions containing 10 mM NaCl background electrolyte strengths.

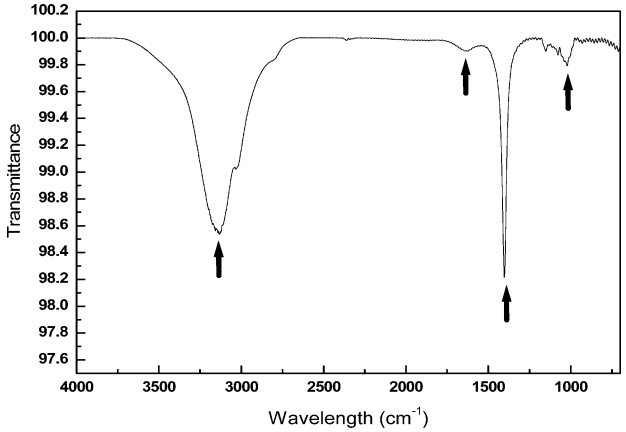

Figure 5. FTIR spectra of starch-coated SPION.

increase in the conductivity observed at pH 12.5. The rapid increase in conductivity was observed at the end of the reaction process. Compared to the conductivity data, the ESA values increased exponentially until 5.98 mPa·M/V at pH = 12.28 and then drastically decreased. The ESA signal was enhanced because the population of SPION increased gradually until the attractive and repulsive forces reached equilibrium at pH 12.28. Excess amounts of SPION in polymeric matrix disturbed the balance of these forces in the reaction solution, resulting in the formation of agglomerate and flocculation.

Figure 4 shows the microelectrophoresis measurements of a dilute suspension of starch-coated SPION. The sample was prepared at high pH (pH = 13) and was constantly stirred overnight before start of the measurements. The pH of the final suspension was decreased by titration with 5×10^{-2} M HCl followed by dispersion with sonication. As shown in Figure 4, an isoelectric point was formed at pH 6.6 for the uncoated SPION in 1×10^{-2} M NaCl background electrolyte. At pH ranges between 4 and 8, the agglomerations of SPION were formed as a consequence of low surface charge density. The highest values of the ξ-potential were observed at high and low pH ranges, most likely due to the hydrodynamic forces introduced by sonication, which were strong enough to prevent the formation of weak bonds. The starch-coated SPION show negative ξ-potentials throughout the entire pH range with the isoelectric point at $pH_{iep} = 2.1$. This result implies that the electrostatic and steric repulsion induced by the starch coating of the SPION were only slightly stronger than those observed for the uncoated SPION at pH around 7−7.5, i.e., the physiological range in the living organisms. However, this colloidal suspension shows stable behavior despite having lower ξ-potential values. This indicated that starch-coated SPION have a flat layer and longer polymeric chains.

FTIR spectral patterns of starch-coated SPION show four peaks at 3137, 1633, 1405, and 1020 cm^{-1} (Figure 5). The absorption regions observed at 3137 and 1633 cm^{-1} were due to the presence of water molecules, and the peak at 1405 cm^{-1} reflects the bending modes of O−C−H, C−C−H, and C−O−H angles. The absorption region at 1020 cm^{-1} relates to C−C and C−O stretching modes of the polysaccharide backbone.

The MRI analysis was performed 1 h after the injection of starch-coated SPION and it showed T_2* signal intensity strongly reduced at all recorded TE values in the gradient-echo images. A more widespread distribution of susceptibility changes was recorded with increasing TE values. Calculated corresponding decreased T_2* values as a consequence of the presence and distribution of SPION around the intrastriatal injection site in the rat brain are shown in Figures 6 and 7. The decreased T_2* values were observed gradually from the center of the injection toward the periphery, indicating a decrease in the concentration of the injected iron oxide nanoparticles.

To confirm the intensity of the transport/diffusion of SPION through the extracellular space in the brain parenchyma, 3D image analysis with MATLAB program was performed (Figure 7b). The starch-coated SPION were effectively transported from the center of the injection site through the extracellular space toward the periphery in the living brain, seen from 3D plotting per unit pixel in Figure 7. The different concentration of SPION in each region shows the signal gradient on T_2* weighted images is due to the difference in magnetic susceptibility. The magnetic susceptibility gradient in a strong magnetic field (4.7 T) shows that SPION are capable to interfere with the proton signals reflecting the distribution of water molecules in the T_2* weighted images of the rat brain.

The morphological evaluation (Figure 8) revealed a large number of middle-sized neurons in the striatum close to the center of the injection site with a prominent appearance of dense, small inclusion bodies in the cytoplasm. The same phenomenon was also observed in the cortex cerebri close to the needle track where a backflow of nanoparticles occurred. No cells with inclusion bodies were observed further out in the cortex.

4. Discussion

Preparation of SPION by Coprecipitation. Because this paper focuses on the transportation of the magnetite nanoparticles in the extracellular space, small particle size and narrow size distribution were preferred. This enabled the particles to have uniform physical and chemical properties. Proper conditions for the preparation of magnetite nanoparticles should be carefully considered and developed for this specific application. The solution chemistry approach to prepare the SPION offers the advantage of small size and narrow size distribution. Magnetite can be obtained by

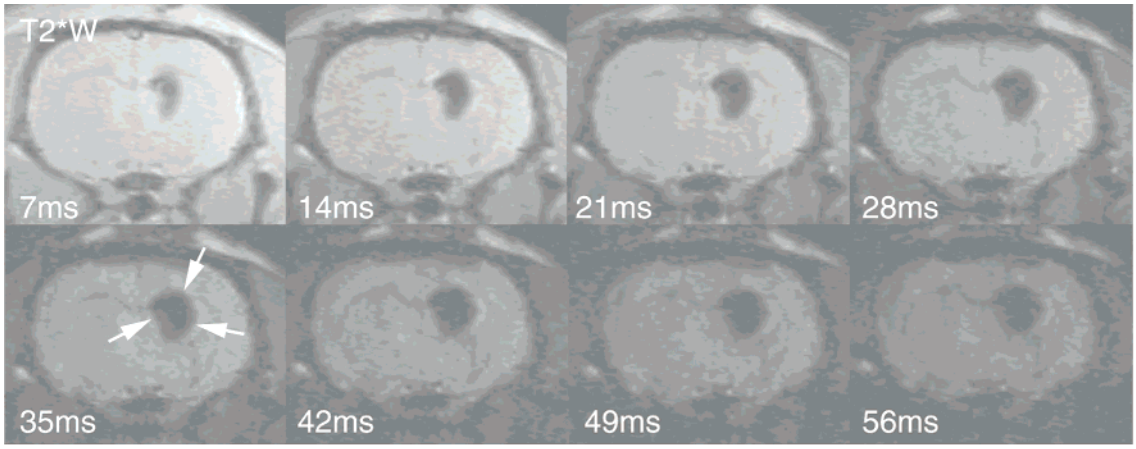

(a)

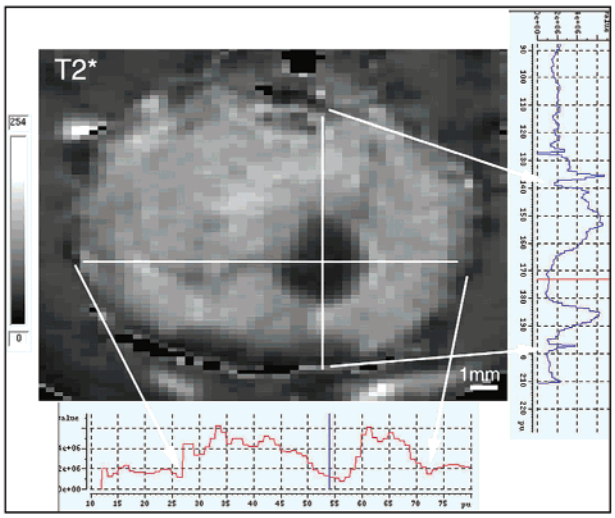

(b)

Figure 6. (a) Series of eight T_2* weighted MR echo images (TE 7−56 ms) indicating a distribution of starch-coated SPION in a coronal section of a living rat brain through the site of injection indicated by arrows. At the center of the injection, the darkest region is found with gradually increasing signal intensity toward the periphery where the amount of SPION decreased. In part b the T_2* values, as calculated from the echo series, are displayed in a gray-scale representation. Image intensities are plotted along the *X* and *Y* axes indicating the susceptibility changes in the brain along the horizontal and vertical indicated lines. Arrows indicate the outer borders of the brain. Scale bar indicates 1 mm.

controlled oxidation of Fe^{2+} in solution. However, the kinetics of oxidation reaction of Fe^{2+} to Fe^{3+} is slow and difficult to control. It is therefore more convenient to control the formation of magnetite by use of a mixture of Fe^{2+} and Fe^{3+} ions in starting solution. In this case, the oxidation step of Fe^{2+} can be omitted.[13] The thermodynamic modeling curves for redox potentials $E = 0$ V and $E = -0.4$ V, respectively, are shown in Figure 9 a and b. In both cases, the complexation of Fe^{2+} with Cl^- in reducing atmosphere was about 50% of Fe^{2+} and takes place at acidic condition, i.e., at pH values up to 4 ($E = 0$ V) and 6 ($E = -0.4$ V). This indicates that either iron chloride or nitrate salts are applicable for the preparation of magnetite. It is also evident that Fe_3O_4 does not form at highly oxidizing conditions, whereas it can be formed as a pure phase during the oxidation of Fe^{2+} in reducing atmosphere within the range of pH 4−6 at $E = 0$ (Figure 9a) or pH 6−13 at $E = -0.4$ V (Figure 9b). It should be mentioned that in our experiments the mole ratio of Fe^{2+}/Fe^{3+} was equal to 1:2. In fact, when the initial Fe^{2+}/Fe^{3+} ratio was 1:2, no impurity phase could be identified by XRD. However, when the reaction was performed at the nonstoichiometric ratio of Fe^{2+}, Fe^{3+}, several impurity phases were formed such as FeOOH, $Fe(OH)_2$, and Fe_2O_3. Therefore, it was shown that the inert atmosphere during the synthesis is important for precipitation of pure magnetite phase. Typically, the pure phase of magnetite appears to be black. When magnetite was coprecipitated without protection from oxygen, the reactants had several iron complexes even though the product color was black. Moreover, some iron complexes have lattice parameters similar to those of magnetite and XRD cannot be used to identify the correct phase. Most reported works did not consider the oxidation mecha-

(13) (a) Kim, D. K. Ph.D. Thesis, Royal Institute of Technology, Stockholm, 2002. (b) Kim, D. K.; Zhang, Y.; Voit, W.; Rao, K. V.; Kehr, J.; Bjelke, B.; Muhammed, M. *Scripta Mater.* **2001**, *44*, 1713.

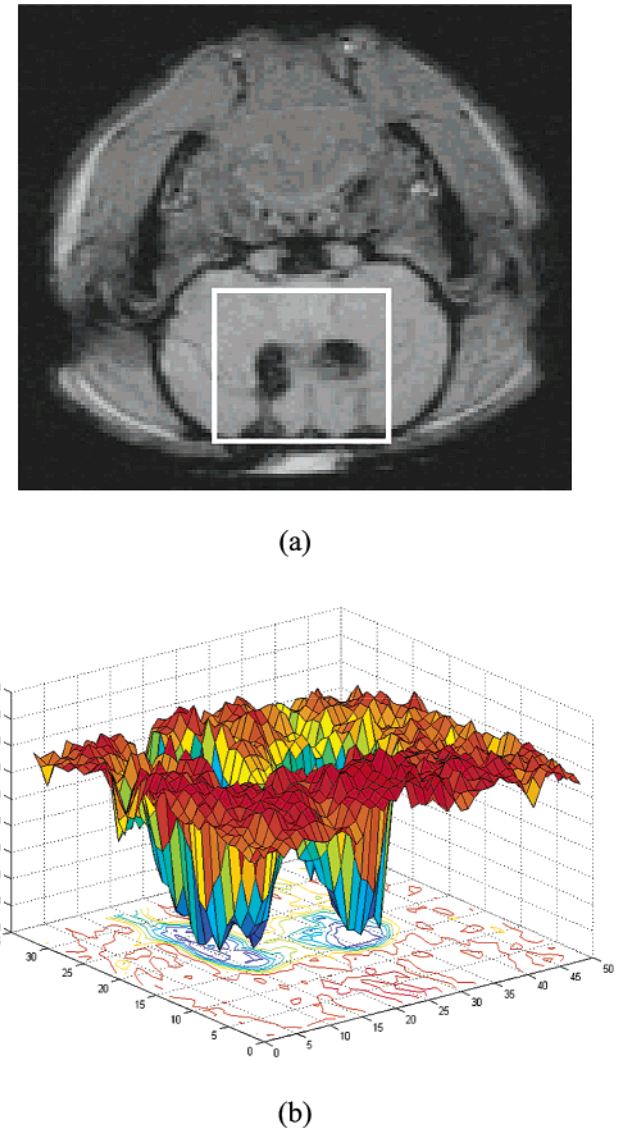

Figure 7. (a) T_2* weighted image indicating the distribution of bilaterally infused starch-coated SPION in a living rat brain (1 h after injection) represented on a gray scale and (b) as signal intensity versus position of the outlined area in (a).

nism of Fe^{2+} by oxygen at ambient atmosphere. When the mixing speed during the precipitation reaction was more than 1000 min^{-1} without flowing N_2 the color of the product turned to brown immediately, which indicated that the phase of the reactant was Fe_2O_3 as a result of strong oxidation. In this work, with a mixing speed of 2000 min^{-1}, N_2 was introduced during the synthesis to protect critical oxidation, which is predicted by thermodynamic modeling of the $Fe^{2+}-Fe^{3+}-Cl^-$ system. The reactant with N_2 flow shows a pure phase magnetite with a strong black color.

Starch-Coated SPION. Normally, the tight junctions permit the diffusion of very small amounts of water-soluble compounds, while the larger surface area of the lipid membranes in the endothelium offers an effective diffusive route for lipid-soluble agents. Also, the endothelium allows protein transport for glucose, amino acids, purine base, and nucleosides, etc. The surface modifications of the SPION with such kinds of biomolecules are demanded for this study. Therefore, starch was selected as a coating agent.

Natural starch is a branched, hydrophilic, and cross-linked polymer that contains 15−30 wt % amylose. Gruber et al.[14] showed that potato starch consists of a core of crystalline amylose surrounded concentrically by a layered shell of amylopectin. These molecules of amylopectin are deposited as fringed folded micelles. The molecules are bound to their neighbors by hydrogen bonds. The outer part of the amylopectin layers is swollen to a certain degree. Some are extended toward the water and loosely connected with other amylopectin molecules. Thus, the swollen starch granules form a three-dimensional scaffold structure. This three-dimensional polymeric matrix should prevent the agglomeration of SPION and keep individual SPION separated during nucleation. The iron oxide particles start to nucleate from the precipitation of Fe^{2+} and Fe^{3+} embedded in the polymeric starch matrix. At a certain critical size, r_n, the increase in free energy due to an increase of surface area is balanced by a decrease in ΔG, due to energy differences between the SPION crystal and surrounding media. This stage represents the end of nucleation and the beginning of growth of the particles.[15]

The starch matrix hinders cluster growth after nucleation due to the reaction between iron cations and hydroxide anions. In addition, the polymer layer on the surface of the SPION prevents further oxidation, which affects the phase transformation during the coprecipitation process. These polymeric networks cover a large number of continuous magnetite monodomains and keep them apart against surface tension forces. Also, to transport this hydrophilic substance in biological membrane systems, surface modifications of the nanoparticles are necessary to adjust the ξ-potential close to zero at pH 7.4. The SPION produced in a starch matrix shows extremely stable behavior for 1 year in aqueous media at room temperature.

Agglomeration of the magnetite nanoparticles is initiated from the collisions between particles for nucleus formation. The collision of particles formed initial agglomerated clusters in the liquid carrier. Growth of the agglomeration is driven by both attraction and capillary forces between the magnetite clusters and single nanoparticles. Nanosized magnetite particles have large surface area and small curvature with the neighbor particles. The large surface energy accelerates the agglomeration process in order to decrease the free energy (ΔG) of the system.

When H_2O_2 was used to cleave the glycosidic bond of the starch molecule, a marked reduction in agglomeration size was observed. However, increased addition of H_2O_2 to starch-coated SPION, i.e., when more than 7.6 $\times$ 10^{-2} M H_2O_2 was added, resulted in an increase of the agglomeration size. An aqueous solution of H_2O_2/NaOH cleaved the glycosidic bonds and reduced the polymeric chains to a critical average molecular weight. Excess amounts of peroxide (sample S6) yield an incomplete shielding, which increases the probability of contact between the particles.

Starch-Coated SPION in the Brain Tissue. Certain proteins, such as insulin and transferrin, are taken

(14) Gruber, V. E.; John, K.; Schurz, J. *Staerke* **1973**, *25*, 109.
(15) Kim, D. K.; Zhang, Y.; Voit, W.; Rao, K. V.; Muhammed, M. *J. Magn. Magn. Mater.* **2001**, *225* (1−2), 30.

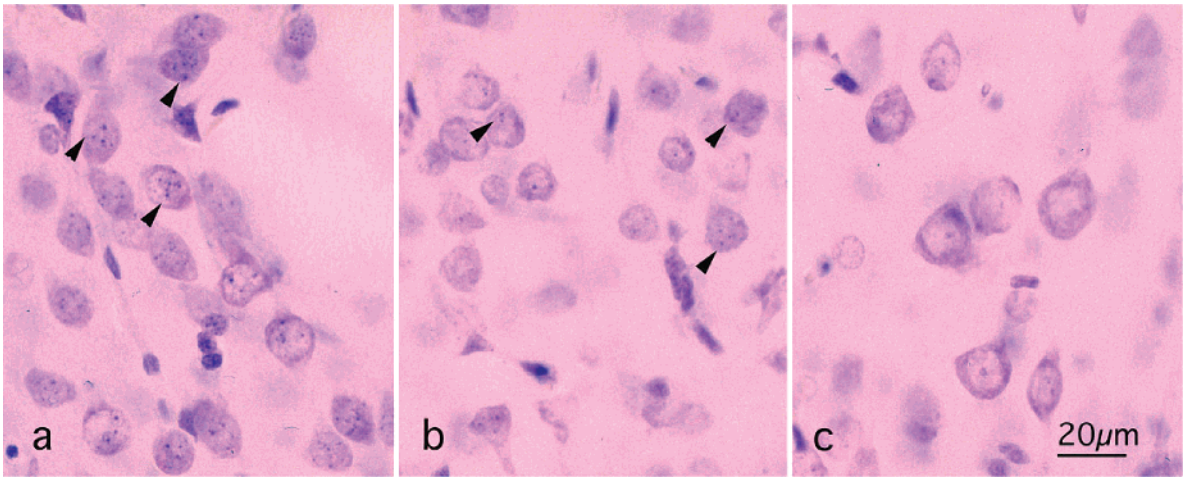

Figure 8. Microphotograph of striatal neurons (panel a) showing inclusion bodies (indicated by arrowheads). Several small, dark, dense vesicles are observed in the cytoplasm. In panel b, the same cytoplasmatic grains-like structures are observed in cortical neurons close to the needle track. The numbers of cells with inclusion bodies are less frequent, and a lesser number of granules per cell is observed. Panel c shows a cortical region, more lateral in the brain where no inclusion bodies are found. Scale bar indicates 20 μm.

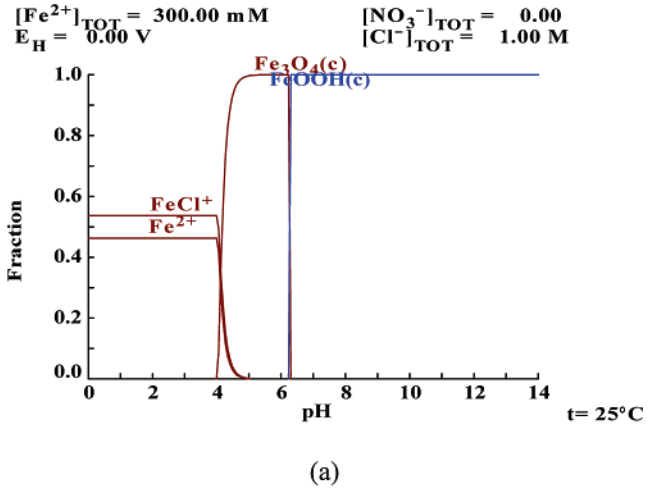

(a)

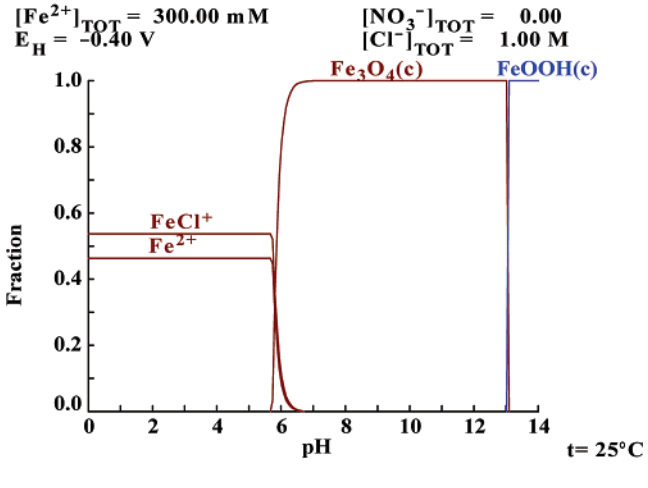

(b)

Figure 9. Thermodynamic modeling diagram showing the distributions of the fraction of $[Fe^{x+}]/[Fe^{2+} + Fe^{3+}]$ vs pH calculated at 25 °C for 0.3 M Fe^{2+} and 1 M Cl^- solution: (a) $E = 0$ and (b) $E = -0.4$ V.

up by specific receptor-meditated endocytosis, whereas most native plasma proteins, such as albumin, are poorly transported across cell membranes. Cationization can increase their uptake by adsorptive endocytosis and transcytosis.[16]

SPION was reported as a liver-specific MRI contrast agent where it is taken up by the Kupffer cells.[17] A number of studies have been reported in the use of the commercially available dextran-coated SPION (Endorem, Guerbert, France) with an agglomeration size between 120 and 250 nm as a MR contrast agent. "Standard" in vivo experiments were performed by infusing the SPION intravenously over 35 min.[18] When the particle size of magnetite is larger than 50 nm, it can be used readily for in vitro magnetic separation of biological samples in suspension. Biomedical applications for neuroresearch using SPION, in vivo, would preferentially require smaller particle size, less than 50 nm, which is the diameter of the reticuloendothelial system (RES) capillary in the brain. The particles should have a narrow size distribution and surface coating with biocompatible materials, i.e., nonimmunogenic, nonantigenic, and protein-resistant. However, the agglomeration of the SPION due to dipole−dipole interaction between the magnetic particles is a potential limitation for biomedical applications.

The influence of surface modifications of the SPION on the diffusion properties of this material within the striatum of the rat brain was evaluated and the internalization of particles into neurons was found. For in vivo administration of SPION, specifically after intravenous or intramuscular injection, a strong phagocytotic uptake of SPION in certain cells has been reported previously.[19]

Infusion of SPION in living rat brain tissue was performed as a preliminary experiment to monitor extracellular macromolecules both at a single cell level, which is relevant for labeling genes and intracellular proteins, and a network level for tracing intercellular

(16) Abbott, N. J.; Romero, I. A. *Mol. Med. Today* **1996**, *2*, 106.
(17) Bellin, M. F.; Zaim, S.; Auberton, E.; Sarfati, G.; Duron, J. J.; Khayat, D.; Grellet, J. *Radiology* **1994**, *193*, 657.
(18) Balci, N. C.; Sirvanci, M.; Duran, C.; Akinci, A. *Clin. Imaging* **2002**, *26*, 35.
(19) Zhang, Y.; Kohler, N.; Zhang, M. *Biomaterials* **2002**, *27*, 1553.

communication. For these specific purposes, SPION were prepared in polymeric starch networks with a particle size about 42 nm (S5), which is smaller than commercially available magnetic nanoparticles.

Starch-coated SPION was directly administrated into the brain parenchyma to study the interaction of SPION in the extracellular compartment of the brain and the active and passive transport routes for CSF which could be expected to be preferential pathways for SPION.[20] The periphery of the injection area clearly appears gradually hypointense with regard to adjacent brain tissue because of the accumulation and diffusion/transport of SPION. Because of the high intrinsic contrast between the injection area and surrounding tissue, morphometric analysis of MR images can be readily carried out. The MRI results imply that for MR imaging with starch-coated SPION, both the image intensity and contrast might be severely amended by the existence of SPION. T_2*-weighted images represent signal intensity changes corresponding to decreasing T_2* values indicating a concentration gradient of starch-coated SPION in the brain tissue. This indicates a gradual decrease of starch-coated SPION from the center of the injection site toward the periphery of the striatum.

On the basis of light microscopic evaluations, it seems likely that not only peptides and dextran,[21] but also nanoparticle, are transported in the extracellular space and also internalized in both striatal and cortical neurons. SPION incorporation into *T*-lymphocytes has previously been reported[22] and was proposed to take place by endocytosis, indicating a possible endocytotic uptake in nerve cells in the brain. Thus, the starch-coated SPION show a biocompatibility and possibility of being transported in the extracellular space as well as being internalized in nerve cells. Further development is needed to determine the surface modification and functionalization in order to prevent or promote the cellular internalization capability of the SPION.

Acknowledgment. This work has been supported by the Swedish Foundation for Strategic Research (SSF), and Swedish Research Council for Engineering Sciences (TFR), Konung Gustaf V:s och Drottning Viktorias Stiftelse.

CM031104M

(20) Bjelke, B.; England, R.; Nicholson, C.; Rice M. E.; Lindberg, J.; Zoli, M.; Agnati, L. F.; Fuxe, K. *NeuroReport* **1995**, *6*, 1005.

(21) Bjelke, B.; Fuxe, K. *NeuroReport* **1993**, *5*, 265.

(22) Yeh, T. C.; Zhang, S. T.; Ildstad, H. C. *Magn. Reson. Med.* **1993**, *30*, 617.